ACS APPLIED MATERIALS & INTERFACES

Research Article

www.acsami.org

Enhanced Lithium Storage Performances of Hierarchical Hollow MoS_2 Nanoparticles Assembled from Nanosheets

Meng Wang,[†] Guangda Li,[†,‡] Huayun Xu,[†] Yitai Qian,[†,§] and Jian Yang*[,†]

[†]Key Laboratory of Colloid and Interface Chemistry, Ministry of Education, and School of Chemistry and Chemical Engineering, Shandong University, Jinan, 250100, P.R. China

[‡]Shandong Polytechnic University, Jinan 250100, P.R. China

[§]Hefei National Laboratory for Physical Science at Microscale and Department of Chemistry, University of Science and Technology of China, Hefei, Anhui 230026, P.R. China

Supporting Information

ABSTRACT: MoS_2, because of its layered structure and high theoretical capacity, has been regarded as a potential candidate for electrode materials in lithium secondary batteries. But it suffers from the poor cycling stability and low rate capability. Here, hierarchical hollow nanoparticles of MoS_2 nanosheets with an increased interlayer distance are synthesized by a simple solvothermal reaction at a low temperature. The formation of hierarchical hollow nanoparticles is based on the intermediate, $K_2NaMoO_3F_3$, as a self-sacrificed template. These hollow nanoparticles exhibit a reversible capacity of 902 mA h g^{-1} at 100 mA g^{-1} after 80 cycles, much higher than the solid counterpart. At a current density of 1000 mA g^{-1}, the reversible capacity of the hierarchical hollow nanoparticles could be still maintained at 780 mAh g^{-1}. The enhanced lithium storage performances of the hierarchical hollow nanoparticles in reversible capacities, cycling stability and rate performances can be attributed to their hierarchical surface, hollow structure feature and increased layer distance of S−Mo−S. Hierarchical hollow nanoparticles as an ensemble of these features, could be applied to other electrode materials for the superior electrochemical performance.

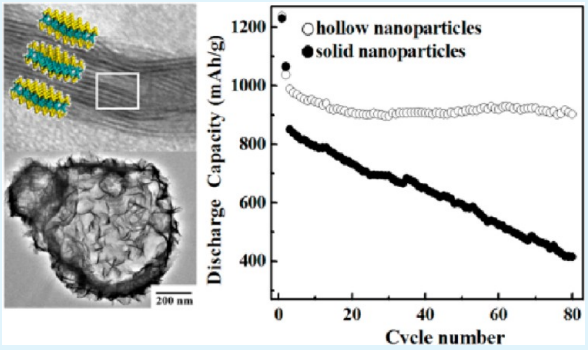

KEYWORDS: *hierarchical surface, hollow structure, layered compounds, nanomaterials, lithium secondary batteries, solvothermal reaction*

INTRODUCTION

Lithium-ion batteries (LIBs), as one of important portable devices for energy storage, have inspired intensive interests in the past decades. Because the practical applications of LIBs strongly depend on the cycling performance and reversible capacity of electrodes, how to improve these performances of electrodes becomes a hot topic to both chemists and material scientists.[1−4] Compared with the commercial anode of LIBs like graphite, MoS_2, also an inorganic graphene analogue,[5,6] is more attractive in terms of its high theoretical specific capacity (∼ 670 mA h g^{-1}, based on 4 mol of Li^+ insertion). Furthermore, the weak interaction between neighboring layers benefits the insertion and extraction of lithium. So, a number of MoS_2 nanoparticles in different morphologies have been fabricated for rechargeable batteries. But their performances suffer a lot from the poor cycling stability and low rate capability. Chen et al. synthesized MoS_2 nanoflowers by an ionic liquid-assisted hydrothermal reaction.[7] The initial specific capacity of the flower-like MoS_2 could be as high as 869 mA h g^{-1}, but the capacity quickly decayed to 633 mA h g^{-1} after 50 cycles at a current of 100 mA g^{-1}. Lou and co-workers prepared hierarchical MoS_2 microspheres that present a comparable reversible capacity at 672 mA h g^{-1} at 100 mA g^{-1} after 50 cycles.[8]

The poor cycling stability and low rate capability could be significantly improved by increasing the interlayer distance of MoS_2 for less strain and smaller intercalation barrier of Li. The strategy has been demonstrated to be successful in restacked MoS_2 prepared by an exfoliation−restacking process,[9] PEO-inserted MoS_2 obtained by the hydrolysis of lithiated MoS_2,[10] carbon-intercalated MoS_2 nanoparticles synthesized by a hydrothermal reaction followed with a high-temperature annealing,[11] and mesoporous MoS_2 achieved by a SBA-15 templated method.[12] The latter two MoS_2 samples even gave a reversible capacity about 900 mA h g^{-1} at a rate of 100 mA g^{-1}. The best performance came from amorphous MoS_2 nanoplates obtained by a solvothermal method. These amorphous MoS_2

Received: November 13, 2012
Accepted: January 18, 2013
Published: January 18, 2013

nanoplates exhibited a reversible specific capacity of 912 mA h g^{-1} at 1060 mA g^{-1} after 50 cycles.[13]

Another strategy for electrodes to achieve good stability and rate capability is to make them the hierarchical hollow nanoparticles, where the hollow structure, nanoscale size and hierarchical organization of building blocks could effectively reduce the volume change during the charge/discharge process, shorten the diffusion distance of Li^+ and increase the active sites for lithium storage.[14−21] However, such hierarchical hollow nanoparticles of MoS_2 have not been explored for lithium storage before, although some hollow MoS_2 nanoparticles have been synthesized in literature.[22] Tremel et al. successfully developed a metal−organic chemical vapor deposition (MOCVD) technique to prepare hollow MoS_2 nanoparticles in the size of 30−50 nm.[23] Li et al. replaced these organometallics with Na_2MoO_4 and conducted the sulfurization reaction by a hydrothermal method, followed with a high-temperature annealing.[24] The hollow MoS_2 nanoparticles could be also achieved by sonochemical deposition on silica powder followed with an etching by hydrofluoric acid.[25] Compared with these hollow nanoparticles, the synthesis for hierarchical hollow structure of MoS_2 is studied to a much lesser extent.[26]

Here, the combination of the two strategies has been realized in the hierarchical hollow nanoparticles of MoS_2 nanosheets with an increased interlayer distance, which are synthesized by a simple solvothermal reaction at a low temperature. The as-prepared hierarchical hollow nanoparticles of MoS_2 are characterized by XRD, SEM, TEM, and HRTEM images for their crystal structure and morphology. The temporal evolution of the products is monitored with TEM images and XRD patterns to disclose the formation mechanism of the hierarchical hollow nanoparticles. Cyclic voltammograms (CV), charge−discharge voltage profiles, cycling and rate performances of these hierarchical hollow nanoparticles are measured to confirm their excellent lithium-storage ability, much better than most of the previous reports. The underlying reasons for the superior lithium-storage performance are also discussed in detail.

EXPERIMENTAL SECTION

Synthesis of Hierarchical Hollow MoS_2 Nanoparticles. In a typical procedure, 0.865 g of molybdenum trioxide (MoO_3, 99.9% purity) powder, 0.515 g of sodium fluoride (NaF, 98.5% purity), and 1.930 g of potassium thiocyanate (KSCN, 98.5% purity) were added to a mixture of 30 mL of distilled water and 10 mL of ethanol. After being stirred for 10 min, the solution was then transferred into a Teflon-lined stainless steel autoclave with a capacity of 50 mL. The autoclave was sealed and maintained at 200 °C for 16 h. The dark precipitates were collected and washed with diluted acid and absolute ethanol several times. Finally, the product was dried under vacuum at 60 °C. To evaluate the performances of these hierarchical hollow nanoparticles in LIBs, the solid MoS_2 nanoparticles were prepared by the similar procedure, using glycerine for the solvent mixture rather than ethanol. The other experiment parameters were kept as the same.

Materials Characterization. The X-ray diffraction (XRD) patterns were obtained on an X-ray diffractometer (D8 Advance, German) equipped with a rotating anode, using graphite-monochromatized Cu Kα as a radiation source. Transmission electron microscope (TEM) images were acquired with a transmission electron microscope of JEM-1011 at an accelerating voltage of 100 kV. High-resolution TEM (HRTEM) images were recorded with an analytic transmission electron microscope of JEOL 2010 at 200 kV. Scanning electron microscope (SEM) images were acquired from a field emission scanning electron microscope (JEOL JSM-7600F). N_2 adsorption−desorption isotherms were measured on a QuadraSorb S1 apparatus at 77 K. The surface areas were calculated by the Brunauer−Emmett−Teller (BET) method.

Electrochemical measurements. The working electrodes were prepared by 70 wt % active materials (MoS_2), 20 wt % carbon black, and 10 wt % poly(vinylidene fluoride) (PVDF) on a copper foil. Then, the coated copper foil was dried under vacuum at 80 °C for 24 h and cut into pieces with a diameter of 12 mm before use. A Celgard 2300 membrane was used as a separator between the working electrode and the counter electrode (Li foil). The electrolyte was 1 M $LiPF_6$ in the mixture of ethylene carbonate/dimethyl carbonate/diethyl carbonate (EC/DMC/DEC, 1:1:1 v/v/v). The working electrode, the separator, the electrolyte, and the counter electrode, were assembled to a coin-type cell (2032) in an argon-filled glovebox (Mikrouna, Super 1220/750/900). Cyclic voltammetry (CV) profiles (0.01−3.0 V, 0.1 mVs^{-1}) were obtained on an electrochemical workstation (CHI 660C, Shanghai, China). Galvanostatic charge/discharge cycles of the cells were conducted between 0.01 and 3.00 V on a LAND CT-2001A battery cycler (Wuhan, China) at room temperature. Electrochemical impedance spectroscopy (EIS) was measured on an FRA-520 (MaterialsMates, Italia) connected to a Potentiostat-510 (MaterialsMates) over the frequency range of 100 kHz to 0.01 Hz.

RESULTS AND DISCUSSION

Figure 1 shows the XRD pattern of the as-obtained product. All the diffraction peaks in the pattern can be indexed as

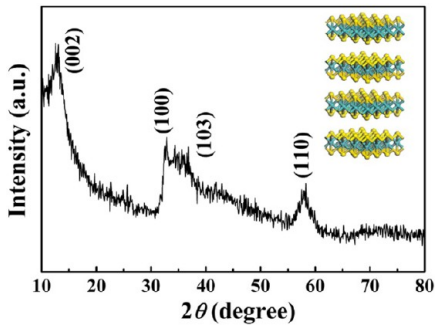

Figure 1. XRD pattern of the hierarchical hollow MoS_2 nanoparticles. The inset shows the lamellar structure of MoS_2 crystals.

hexagonal-phase MoS_2 (JCPDS No. 37−1492). No diffraction peaks from impurities are observed in the XRD pattern. The lattice constants of MoS_2 calculated from this XRD pattern are a = 3.16 Å and c = 12.76 Å. The former is very close to the standard value of MoS_2 (a = 3.16 Å), but the latter shows an obvious increase in comparison with that of MoS_2 (c = 12.29 Å). The results indicate that the distance between neighboring MoS_2 layers increases but their in-plane structure is preserved. The increasing of the layer distance might be associated with the strain/stress caused by the bending and folding of the layers. This increasing of the layer distance would facilitate the diffusion of lithium ions during the insertion/extraction processes. Based on the Scherrer formula, the dimension of the product along z-axis is 52.78 Å, corresponding to approximate 8 layers of MoS_2. This result is in good agreement with that observed in HRTEM images.

The size, shape, and structure of the as-prepared MoS_2 are characterized by SEM and TEM microscopy. As shown in Figure 2a, the as-prepared MoS_2 consists of many spherical nanoparticles with their diameter of 300−800 nm. The nanoparticles show a relatively broad size distribution, which could be attributed to the absence of any surfactants in the reaction. The surface of the nanoparticles is highly wrinkled, which would greatly benefit the increase in the contacting area

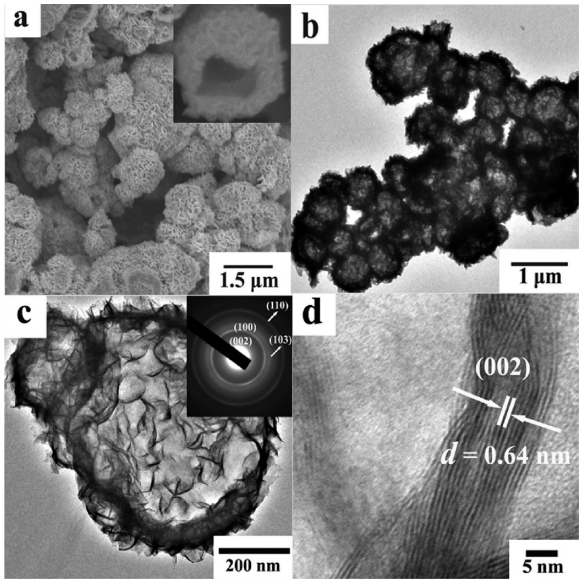

Figure 2. (a) SEM image, (b, c) TEM images, and (d) HRTEM image of the hierarchical hollow MoS_2 nanoparticles. Inset of a shows a broken MoS_2 hollow nanoparticle; inset of c shows the corresponding SAED pattern.

between the electrolyte and electrode material and then promote the insertion/extraction of lithium. Some of the nanoparticles are broken, exposing a hollow interior (the inset in Figure 2a). Figure 2b shows a typical TEM image of the nanoparticles. In this figure, each particle presents a significant contrast between the edge and center, confirming the hollow structure feature again. Figure 2c shows a typical high-magnification TEM image of a single hollow nanoparticle. The highly wrinkled surface and extruded lamella on the shell indicates that the hollow nanoparticles are probably composed of MoS_2 nanosheets. They are folded, curved and assembled into the hierarchical hollow nanoparticles. The hierarchical surface and hollow structure would offer a huge specific surface area for electrochemical reactions, which has been confirmed by BET analysis. As indicated by Figure S1 in the Supporting Information, the specific surface area of the hierarchical hollow nanoparticles could be as high as 138 $m^2\ g^{-1}$. The selected-area electron diffraction (SAED) pattern of the hollow nanoparticle displays several bright diffraction rings that could be indexed as the (002), (100), (103), and (110) reflections of hexagonal-phase MoS_2, as presented in the inset of Figure 2c. The HRTEM image of a hollow nanoparticle (Figure 2d) shows that the nanosheets consist of 5−10 S−Mo−S layers. The distance between adjacent layers is ∼0.64 nm, slightly larger than the reported data (0.62 nm) for the (002) planes of MoS_2, which is consistent with the results obtained from the XRD pattern. EDS spectrum of the hollow nanoparticles (see Figure S2 in the Supporting Information) gives the signals of Mo and S, besides Cu. The molar ratio of Mo:S is about 1:1.85, close to the stoichiometric ratio of MoS_2.

To disclose the formation mechanism of the hollow MoS_2 particles, the reaction process is followed by XRD, TEM, and EDS techniques. In a typical procedure, the reaction was stopped at different times (4, 8, 12, and 16 h) and the products were collected from the solution by centrifugation. The products were then used for XRD patterns and TEM images without any washing. As shown in Figure 3a, the product after reacted for 4 h, is composed of solid particles with a smooth

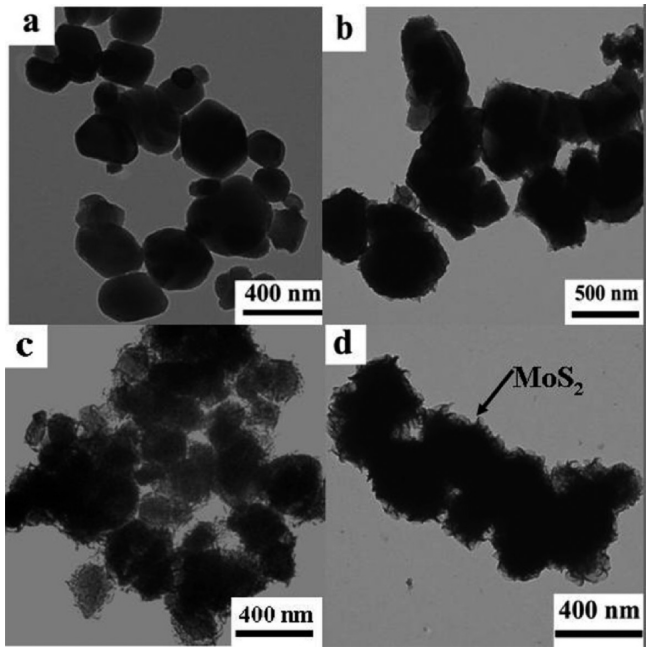

Figure 3. Typical TEM images of as-synthesized products obtained at different times without any post-treatment: (a) 4, (b) 8, (c) 12, and (d) 16h.

surface. The XRD pattern (see Figure S3 in the Supporting Information) indicates the product can be identified as $K_2NaMoO_3F_3$ (JCPDS No. 74−0297) resulted from the reactions between MoO_3, NaF and K^+. EDS spectrum evidences the absence of sulfur in the product. After 8 h, the XRD pattern of the product is almost the same as that obtained at 4 h. But some extruded lamella appears on the surface of the solid particles, as shown in Figure 3b. The rough surface of the particles could be easily visualized in the products obtained at 12 and 16 h (Figure 3c, d). Meanwhile, the content of sulfur in the products at 8, 12, and 16 h gradually increases from 7.21% to 19.87 and 46.65%, respectively. The HRTEM image (see Figure S4 in the Supporting Information) of the product further confirms the formation of MoS_2 sheets on the surface, where sulfur must comes from the decomposition of SCN^-. After the removal of $K_2NaMoO_3F_3$ with diluted acid and absolute ethanol, the product is dominant by the hollow MoS_2 nanoparticles, as shown in Figure 1 and Figure 2. So, it is believed that the formation of the hollow MoS_2 particles can be concluded with $K_2NaMoO_3F_3$ as a self-sacrificed template (Scheme 1). The similar process has also been reported in the synthesis of cubic microcages built by bilayer-structured MoS_2.[26]

The electrochemical properties of the hierarchical hollow nanoparticles are investigated with a Li foil as the counter and reference electrode. Figure 4a shows the typical cyclic voltammograms (CVs) of these hierarchical hollow nanoparticles, which are basically consistent with literature.[13,7,8,27]

Scheme 1. Formation Process of Hierarchical Hollow MoS_2 Nanoparticles

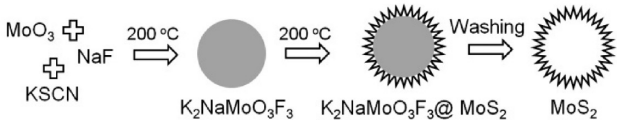

dx.doi.org/10.1021/am3026954 | ACS Appl. Mater. Interfaces 2013, 5, 1003−1008

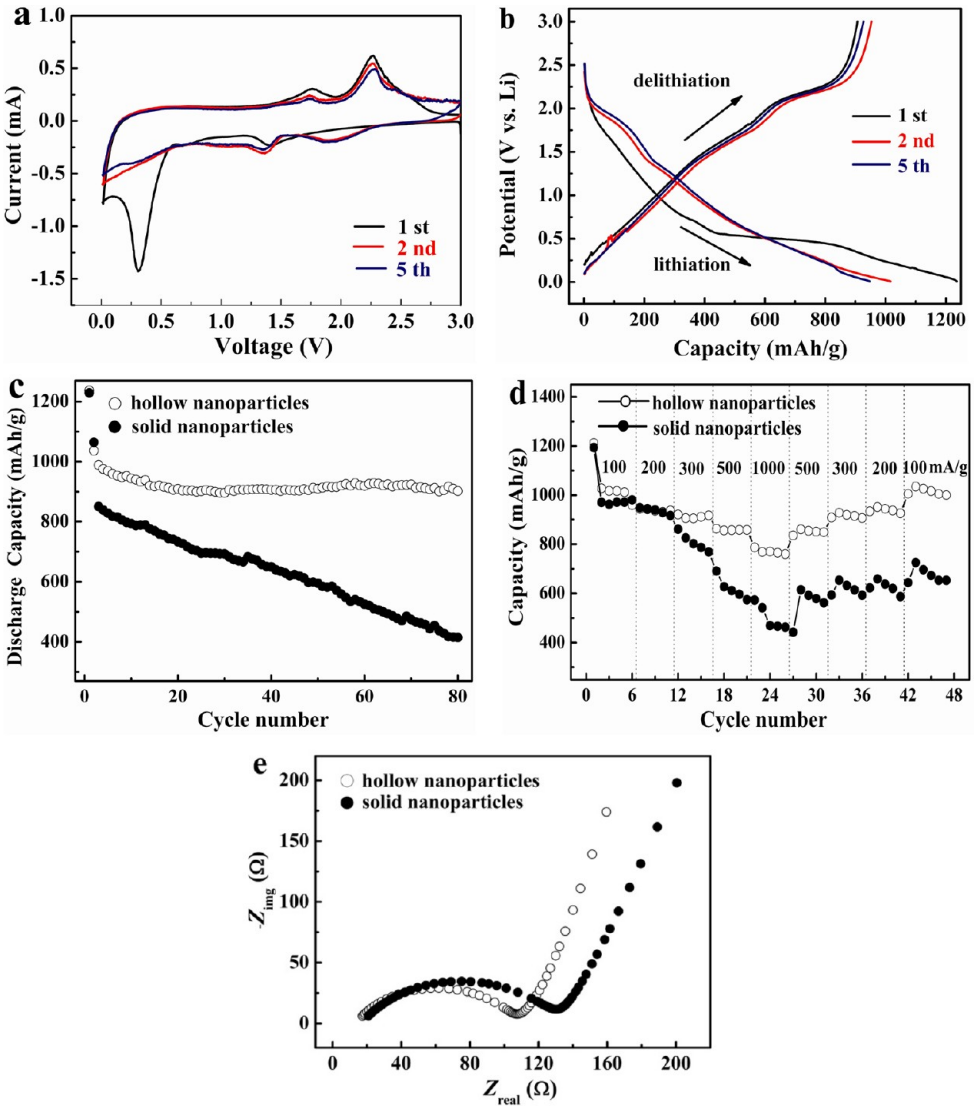

Figure 4. (a) Cyclic voltammograms of the hierarchical hollow MoS_2 nanoparticles at a scan rate of 0.1 mV s^{-1}; (b) discharge/charge voltage curves of the hierarchical hollow MoS_2 nanoparticles at a current density of 100 mA g^{-1}; (c) cycling stabilities of the hierarchical hollow MoS_2 nanoparticles (empty circles) and the solid MoS_2 nanoparticles (solid circles) at a rate of 100 mA g^{-1}; (d) rate performances of the hierarchical hollow MoS_2 nanoparticles (empty circles) and the solid MoS_2 nanoparticles (solid circles) in the voltage range of 0.01−3 V; (e) Nyquist plots of the electrodes at open-circuit voltage.

The first cathodic peak centered around 1.40 V can be attributed to the insertion of Li into the interlayers of MoS_2, resulting from the formation of Li_xMoS_2 due to the transformation of coordination polyhedron of Mo from a trigonal prism to an octahedron.[12,28−30] The intense cathodic peak at approximately 0.30 V is indicative of the conversion of Li_xMoS_2 into metallic Mo and Li_2S. In the later cathodic sweeps, the emergence of a new peak at 1.90 V indicates the formation of a gel-like polymeric layer.[9,27,30] During the anodic scans, two peaks at 1.78 and 2.30 V are clearly observed and maintained for the subsequent sweeps. But there are intense arguments about the origin of the two peaks. Most of the previous reports explain the peaks as the oxidation of Mo to MoS_2.[8,9,31] Then, the lithium-storage mechanism can be described with the following reaction:

$$MoS_2 + 4Li \leftrightarrow Mo + 2Li_2S \quad (1)$$

Unfortunately, these reports did not give any evidence from the electrodes after discharge or charge to support this mechanism. Recently, the mechanism is questioned in view of XRD patterns and TEM images from the electrodes after discharge and charge.[29,32,33] For example, Wang and co-workers reported the XRD patterns and TEM images of the MoS_2 electrode after discharge and charge, confirming the appearance of sulfur in the electrodes after recharge. Shi and Hu got the same conclusion, based on the polarization between the cathodic peaks and the corresponding anodic ones. These results imply that Li_2S is likely to be oxidized into S during the anodic scans. Thus, the lithium-storage mechanism can be expressed by the next reaction

$$S + 2Li \leftrightarrow Li_2S \quad (2)$$

Figure 4b shows the discharge−charge profiles of the hierarchical hollow MoS_2 nanoparticles for first, second and fifth cycle at a current density of 100 mA g^{-1}. The initial lithiation (discharge) and delithiation (charge) capacities of these hierarchical hollow nanoparticles are 1236 and 907 mA h g^{-1}, corresponding to a Coulombic efficiency of 74%. The

dx.doi.org/10.1021/am3026954 | ACS Appl. Mater. Interfaces 2013, 5, 1003−1008

capacity loss might arise from the irreversible reactions during the discharge/charge processes, such as the formation of solid electrolyte interphase (SEI) and/or some lithium trapping inside the lattice.[9,31] As presented in Figure 4c, the discharge capacity of the hierarchical hollow MoS_2 nanoparticles could be still maintained at 902 mA h g^{-1} even after 80 cycles, much higher than that of solid MoS_2 nanoparticles at 410 mA h g^{-1} (see Figure S5 in the Supporting Information). These solid and rough MoS_2 nanoparticles in a size of 200−700 nm are prepared by the similar procedure. The data reported here are higher than most of the reported works. Lou et al. reported that hierarchical MoS_2 spheres synthesized by the assistance of polystyrene, displayed the specific capacities of 672 mA h g^{-1} after 50 cycles and 585 mA h g^{-1} after 70 cycles at a current of 100 mA g^{-1}.[8] Guo et al. found that restacked MoS_2 prepared by the exfoliation and restacking process exhibited a reversible capacity of 750 mA h g^{-1} at 50 mA g^{-1} after 50 cycles.[9] A similar result came from the flowerlike MoS_2 particles obtained in ionic liquids, which showed a specific capacity of 633 mA h g^{-1} at a current density of 100 mA g^{-1} after 50 cycles.[7] The high specific capacity and superior cycling stability of the hierarchical hollow nanoparticles could be attributed to their large specific surface area, hollow structural feature and increased layer distance of S−Mo−S.[8,9,12,13] The large surface area indicates the increased reactive sites and interfaces, and then favors the active material to achieve a high specific capacity. The hollow structure could effectively tolerate the volume change caused by the discharge/charge processes, reduce the diffusion distance of lithium ions, and then improve the cycling stability. The increased layer distance between neighboring S−Mo−S layers would facilitate the quick diffusion of lithium ions and improve the reaction reversibility.

As a result of these advantages, the hierarchical hollow nanoparticles exhibit a better rate performance than the solid ones, as shown in Figure 4d. At the current densities of 100, 200, 300, 500, and 1000 mA g^{-1}, the specific capacities of the hierarchical hollow MoS_2 nanoparticles are 1030, 950, 910, 850, and 780 mA h g^{-1}, respectively. When the current density goes back to 100 mA g^{-1}, the specific capacity of the hierarchical hollow MoS_2 nanoparticles also returns to 1010 mA h g^{-1}, indicating the good rate capability of the active material. The data reported here are higher than most of the reported works. The hierarchical MoS_2 microspheres obtained with poly styrene as the templates showed the specific capacities of 581 mA h g^{-1} for 500 mA g^{-1} and 353 mA h g^{-1} for 1000 mA g^{-1}.[8] Restacked MoS_2 fabricated by the exfoliation and restacking process delivered a reversible capacity of 710 mA h g^{-1} for 1000 mA g^{-1}.[9] MoS_2 nanosheets coated on carbon nanotubes exhibited the specific capacities of 459 mA h g^{-1} for 500 mA g^{-1} and 369 mA h g^{-1} for 1000 mA g^{-1}.[28] The PEO/MoS_2/Graphene composites showed the specific capacities of 520 mA h g^{-1} for 530 mA g^{-1} and 480 mA h g^{-1} for 1000 mA g^{-1}.[32]

Electrochemical impedance spectra (EIS) are measured to reveal why the hierarchical hollow nanoparticles of MoS_2 show the excellent electrochemical performance, as shown in Figure 4e. The Nyquist plots of the hierarchical hollow nanoparticles based on area normalization consist of a semicircle at the high-to-medium frequency region followed by a slope line at the low frequency region. The former is related with the charge transfer resistance (R_{ct}) between electrolyte and electrodes. The latter represents the Warburg impendence (Z_w) caused by the lithium diffusion in electrodes. It is found that the charge transfer resistance of the hierarchical hollow nanoparticles is smaller than that of the solid counterpart, which might be attributed to the increased interlayer-distance and hollow structure in our case.

CONCLUSION

A simple solvothermal reaction at a low temperature has been developed for hierarchical hollow nanoparticles of MoS_2 assembled by nanosheets with an improved lithium storage performance. The crystal structure and morphology of these hierarchical hollow nanoparticles have been characterized by XRD patterns, SEM, TEM, and HRTEM images. Meanwhile, XRD patterns and TEM images indicate that the formation of the hierarchical hollow nanoparticles is through the intermediate product, $K_2NaMoO_3F_3$, as a self-sacrificed template. The hollow nanoparticles deliver a specific capacity of 902 mA h g^{-1} at 100 mA g^{-1} after 80 cycles, much higher than the solid counterpart. Even at a rate of 1000 mA g^{-1}, the reversible capacity of the hierarchical hollow nanoparticles is still kept at 780 mA h g^{-1}. The improved lithium storage performance of the hierarchical hollow nanoparticles than the solid counterpart, can be attributed to their increased layer distance of S−Mo−S, hierarchical surface and hollow structure. It is believed that hierarchical hollow nanoparticles, as an ensemble of these features, offer a possible pathway to enhance the electrochemical performance of other electrode materials.

ASSOCIATED CONTENT

Supporting Information

Nitrogen adsorption−desorption isotherm of hierarchical hollow MoS_2 nanoparticles; EDS spectrum of the hierarchical hollow MoS_2 spheres; XRD pattern and HRTEM image of the intermediate product ($K_2NaMoO_3F_3$@MoS_2) without any treatment; SEM and TEM images of solid MoS_2 nanoparticles. This material is available free of charge via the Internet at http://pubs.acs.org./.

AUTHOR INFORMATION

Corresponding Author

*E-mail: yangjian@sdu.edu.cn. Fax/Tel: +86-531-88364489.

Notes

The authors declare no competing financial interest.

ACKNOWLEDGMENTS

This work was supported by the 973 Project of China (2011CB935901), Natural Science Foundation of China (91022033, 21071055, 51172076, 21203111), New Century Excellent Talents in University (NCET-10-0369), Shandong Provincial Natural Science Foundation for Distinguished Young Scholar (JQ201205), Independent Innovation Foundations of Shandong University (2012 ZD007), and New Faculty Start-up funding in Shandong University.

REFERENCES

(1) Chan, C. K.; Peng, H.; Liu, G.; McIlwrath, K.; Zhang, X. F.; Huggins, R. A.; Cui, Y. *Nat. Nanotechnol.* **2008**, *3*, 31−35.
(2) Han, T. H.; Lee, W. J.; Lee, D. H.; Kim, J. E.; Choi, E. Y.; Kim, S. O. *Adv. Mater.* **2010**, *22*, 2060−2064.
(3) Manthiram, A. *J. Phys. Chem. Lett.* **2011**, *2*, 176−184.
(4) Kovalenko, I.; Zdyrko, B.; Magasinski, A.; Hertzberg, B.; Milicev, Z.; Burtovyy, R.; Luzinov, I.; Yushin, G. *Science* **2011**, *334*, 75−79.
(5) Benavente, E.; Ana, M. A. S.; Mendizabal, F.; Gonzalez, G. *Coord. Chem. Rev.* **2002**, *224*, 87−109.
(6) Tenne, R. *Angew. Chem., Int. Ed.* **2003**, *42*, 5124−5132.

(7) Li, H.; Li, W. J.; Ma, L.; Chen, W. X.; Wang, J. M. *J. Alloys Compd.* **2009**, *471*, 442−447.
(8) Ding, S. J.; Zhang, D. Y.; Chen, J. S.; Lou, X. W. *Nanoscale* **2012**, *4*, 95−98.
(9) Du, G. D.; Guo, Z. P.; Wang, S. Q.; Zeng, R.; Chen, Z. X.; Liu, H. K. *Chem. Commun.* **2010**, *46*, 1106−1108.
(10) Xiao, J.; Choi, D. W.; Cosimbescu, L.; Koech, P.; Liu, J.; Lemmon, J. P. *Chem. Mater.* **2010**, *22*, 4522−4524.
(11) Chang, K.; Chen, W. X.; Ma, L.; Li, H.; Li, H.; F. Huang, H.; Xu, Z. D.; Zhang, Q. B.; Lee, J. Y. *J. Mater. Chem.* **2011**, *21*, 6251−6257.
(12) Liu, H.; Su, D. W.; Zhou, R. F.; Sun, B.; Wang, G. X.; Qiao, S. Z. *Adv. Energy Mater.* **2012**, *2*, 970−975.
(13) Hwang, H.; Kim, H.; Cho, J. *Nano Lett.* **2011**, *11*, 4826−4830.
(14) Lai, X. Y.; Halpert, J. E.; Wang, D. *Energy Environ. Sci.* **2012**, *5*, 5604−5618.
(15) Zhou, L.; Zhao, D. Y.; Lou, X. W. *Angew. Chem., Int. Ed.* **2012**, *51*, 239−241.
(16) Zhu, J. X.; Shi, W. H.; Xiao, N.; Rui, X. H.; Tan, H. T.; Lu, X. H.; Hng, H. H.; Ma, J.; Yan, Q. Y. *ACS Appl. Mater. Interfaces* **2012**, *4*, 2769−2774.
(17) Wang, Q. H.; Jiao, L. F.; Han, Y.; Du, H. M.; Peng, W. X.; Huan, Q. N.; Song, D. W.; Si, Y. C.; Wang, Y. J.; Yuan, H. T. *J. Phys. Chem. C* **2011**, *115*, 8300−8304.
(18) Wang, X.; Wu, X. L.; Guo, Y. G.; Zhong, Y. T.; Cao, X. Q.; Ma, Y.; Yao, J. N. *Adv. Funct. Mater.* **2010**, *20*, 1680−1686.
(19) Xiong, Q. Q.; Tu, J. P.; Lu, Y.; Chen, J.; Yu, Y. X.; Qiao, Y. Q.; Wang, X. L.; Gu, C. D. *J. Phys. Chem. C* **2012**, *116*, 6495−6502.
(20) Zheng, S. F.; Hu, J. S.; Zhong, L. S.; Song, W. G.; Wan, L. J.; Guo, Y. G. *Chem. Mater.* **2008**, *20*, 3617−3622.
(21) Zhou, X. S.; Yin, Y. X.; Wan, L. J.; Guo, Y. G. *J. Mater. Chem.* **2012**, *22*, 17456−17459.
(22) Li, G. W.; Li, C. S.; Tang, H.; Cao, K. S.; Chen, J.; Wang, F. F.; Jin, Y. *J. Alloys Compd.* **2010**, *501*, 275−281.
(23) Etzkorn, J.; Therese, H. A.; Rocker, F.; Zink, N.; Kolb, U.; Tremel, W. *Adv. Mater.* **2005**, *17*, 2372−2375.
(24) Li, X. L.; Li, Y. D. *J. Phys. Chem. B* **2004**, *108*, 13893−13900.
(25) Dhas, N. A.; Suslick, K. S. *J. Am. Chem. Soc.* **2005**, *127*, 2368−2369.
(26) Ye, L. N.; Wu, C. Z.; Guo, W.; Xie, Y. *Chem. Commun.* **2006**, 4738−4740.
(27) Wang, Q.; Li, J. H. *J. Phys. Chem. C* **2007**, *111*, 1675−1682.
(28) Ding, S. J.; Chen, J. S.; Lou, X. W. *Chem.—Eur. J.* **2011**, *17*, 13142−13145.
(29) Fang, X. P.; Yu, X. Q.; Liao, S. F.; Shi, Y. F.; Hu, Y. S.; Wang, Z. X.; Stucky, G. D.; Chen, L. Q. *Micropor. Mesopor. Mat.* **2012**, *151*, 418−423.
(30) Zhou, X. S.; Wan, L. J.; Guo, Y. G. *Nanoscale* **2012**, *4*, 5868−5871.
(31) Chang, K.; Chen, W. X. *J. Mater. Chem.* **2011**, *21*, 17175−17184.
(32) Xiao, J.; Wang, X. J.; Yang, X. Q.; Xun, S. D.; Liu, G.; Koech, P. K.; Liu, J.; Lemmon, J. P. *Adv. Funct. Mater.* **2011**, *21*, 2840−2846.
(33) Fang, X. P.; Guo, X. W.; Mao, Y.; Hua, C. X.; Shen, L. Y.; Hu, Y. S.; Wang, Z. X.; Wu, F.; Chen, L. Q. *Chem. Asian J.* **2012**, *7*, 1013−1017.